Characterization and testing of solid particles to be used in CSP plants: aging and fluidization tests

Minerva Díaz Heras[1], Alejandro Calderón[2], Mónica Navarro[2], J.A. Almendros-Ibáñez[1,3], A. Inés Fernández[2], C. Barreneche[2,*]

[1] Renewable Energy Research Institute, Section of Solar and Energy Efficiency, Albacete, Spain
[2] Dept. of Materials Science & Physical Chemistry, Universitat de Barcelona, Barcelona, Spain.
[3] E.T.S. de Ingenieros Industriales de Albacete, Castilla-La Mancha University, Albacete, Spain
*Corresponding author e-mail: c.barreneche@ub.edu

Abstract

The main limitation of Concentrated Solar Power (CSP) is its maximum operating temperature, since the main fluid used as heat transfer fluid (HTF) and thermal storage media (TES) is molten salts, which degrade around 565 ºC. Therefore, there is great interest in developing HTFs that allow the maximum working temperature to be increased to more than 565 ºC. This increase in the maximum operating temperature of the HTFs will, in turn, allow CSP plant efficiency to be enhanced. Different studies have proposed using particles as a medium to capture and store solar energy, but very little is known about the effect on the particles after resisting several cycles of cooling and heating and what happens to the particles' physical properties when they are fluidized. It is true that a variety of solid particles permit high performance to be achieved at high temperatures and with low material costs, but not all particles are valid for this purpose. This work focuses on different materials considered promising candidates for use as alternative HTF and storage materials in CSP plants, which were characterized and tested: sand, carbo Accucast ID50 and silicon carbide. The properties of the particles before and after being fluidized (assessing their resistance to abrasion) and before and after high temperature (900 ºC) thermal treatments (aging treatment) are the main finding of this paper. This work highlights the considerable advantages of SiC and carbo over sand. This study also determines that the combination of high temperature and several hours of fluidization does not affect the diameter of the particles: However, the fluidized samples vary considerably in diameter. In this way, SEM and DSC techniques highlight the problem of the fine appearance associated with sand during fluidization.

1. Introduction

The enormous growth in the world population, the depletion and increase in the cost of fossil resources, and the acceleration of the effects of climate change are indicators of the need for a change in the current global energy model. Hence, in the coming years, the world will need to achieve better energy efficiency across all the existing energy sources; in other words, the energy shift towards a sustainable model is already here [1]. This need is generating new uncertainties: geopolitical influences on energy development and the growing political restrictions of carbon dioxide (CO_2) emissions, which could impose changes in the future use of energy. Therefore, the world is going to need all possible economic and environmentally responsible energy sources in the forthcoming decades [2- 3].

For all these reasons, it is clear that renewable energy has an outstanding role for the future. Shifting to renewable energy would help us meet the dual goals of reducing greenhouse gas emissions and ensuring reliable, timely, and cost-efficient delivery of energy. According to a recent report from the International Energy Agency [3], the share of renewable energy in global power generation will increase from 29% today to 30% in 2024.

Concentrating solar power (CSP) plants are able to concentrate thermal radiation from the sun's rays to heat up the ray's receiver in the system to very high temperatures [4] and thus produce solar thermal electricity (STE). STE presents advantages in contrast with photovoltaics, since CSP can be installed in combination with thermal storage capabilities. CSP plants have the capacity to continue producing electricity on cloudy days, after sundown, or in the early morning. A total of 5.5 GW were installed in 2018 to produce electricity in CSP plants. This number is 11% higher than the previous year, led by China and Morocco, and is expected to double in 2022. It is worth noting that almost all new CSP plants are expected to be installed with thermal storage systems [5].

Therefore, CSP has many possibilities in the near future. According to the *International Energy Agency,* by 2050, with appropriate support, CSP could provide 11.3 % of global electricity, with 9.6 % from solar power and 1.7 % from backup fuels (fossil fuels or biomass) [4]. Several configurations have been developed for CSP plants [6], with one of the newest being the free-falling particle configuration, which consists of spherical solid particles that are directly heated on the upper side of the tower. These then fall down through the direct radiation of a concentrated sunlight beam [7-8]. A significant advantage of particle receivers is that the particles can be irradiated directly, while with other technologies that use gas or liquid, such as TES media, they cannot [7]. Solid particles are released through a slot at the base of a hopper above the receiver, producing a curtain of particles falling through the receiver [8]. Thenceforth, the particles may be stored for the power cycle [9] in an insulated tank and/or used to heat a secondary working fluid (for example air or steam) by fluidizing the solid particles. Other configurations combine the use of a beam-down reflector with an open fluidized bed [10]. In this case, the solar radiation is directly concentrated on the top of the bed of particles [11, 26], which suffer high abrasion processes due to the high temperatures and the fluidization process.

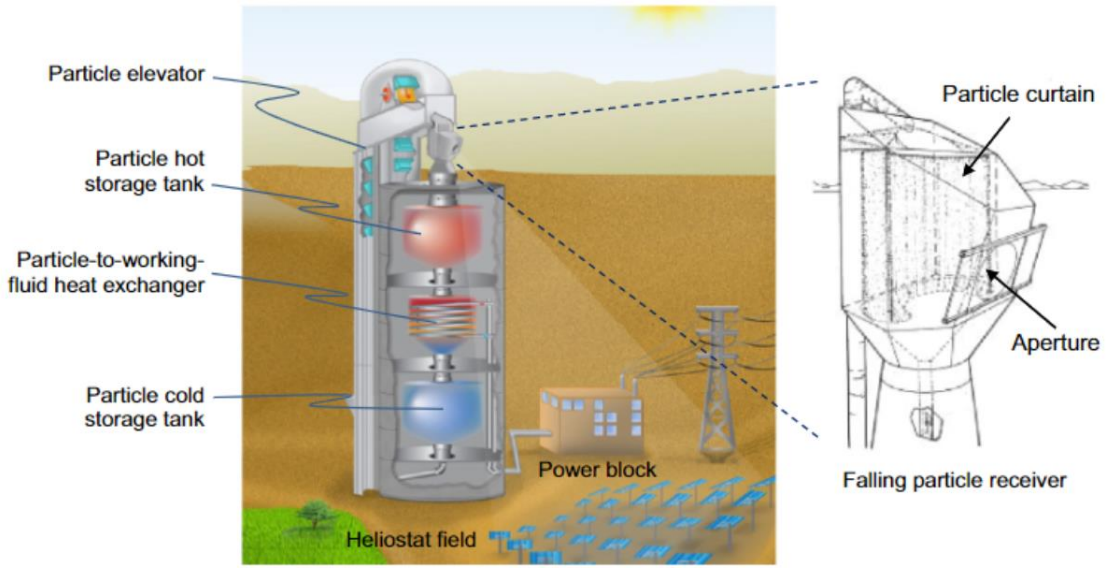

Figure 1: Key parts of a particle receiver [8].

With this technology, temperatures are able to theoretically reach more than 1000 °C without changing the storage material composition and structure, while high receiver efficiency can also be achieved due to direct solar absorption [8-12,26]. Figure 1 shows the free-falling receiver conceptualized by *Sandia National Laboratories* [8-13]. Although a number of analytical and laboratory prior studies on the falling particle receiver were performed, the first set of on sun-tests of a simple particle receiver was also performed by *Sandia National Laboratories* [13]. An alternative concept consists of concentrating the solar radiation on the top of a bubbling fluidized bed with a secondary reflector. This concept was first experimentally tested by Flamant et al. [27,28] in the early 80's, who corroborated the advantage of using a fluidized bed, in comparison to a packed bed, as the appropriate particle technology to rapidly distribute the concentrated solar energy on the top through the whole bed of particles [29]. In recent years, there has been new research using fluidized beds as a system able to capture concentrated solar energy for thermal energy storage [26, 30, 31]. Diaz-Heras et al. [26] tested the same materials studied in this work in a bubbling fluidized bed and observed that SiC presents the highest thermal efficiency during the charging process, although sand obtained lower pumping costs. Tregambi et al. [30] observed the temperature distribution on the top of a directly-irradiated fluidized bed and studied the temperature reduction on the particles generated by bubble injection in the bed. Finally, Sánchez-González and Gómez-Hernández [31] proposed a linear system with Fresnel reflectors, in which the fluidized particles are transported linearly. This allowed them to avoid the problem of the high temperatures the secondary reflector is required to support.

Since the best material for solid particle media for CSP is still unknown, the aim of this paper is to compare three different solid particle materials for this purpose, all of which are reported as suitable candidates in the literature [14-15]. These three proposed materials are SiC [16], silica sand [17], and *Carbo Accucast ID50* [18-19]. They all present, a priori, good properties for high-temperature applications with a fluidized bed. They can resist temperatures above 1000 ºC without chemical changes and have a particle size and density that makes them appropriate for fluidization. They belong to Geldart B particles [32], which can be easily fluidized with a vigorous bubbling that helps to increase the high mixing rates in fluidized beds. In addition, the three materials have previously been tested with satisfactory results in a fluidized bed with a beam-down reflector for thermal energy storage applications [26], with temperatures up to 250 ºC.

Therefore, the main aim of this work is to characterize changes produced in solid particles' composition, structure, or properties when they are brought through several thermal and mechanical processes. The goal is to observe these changes in their physical, thermal and optical properties and also to study the changes in their chemical composition.

2. Materials and treatments

2.1. Solid particles materials

The three selected materials for this study are: Carbo Accucast ID50, Silicon Carbide (SiC) and silica sand (see Figure 2). These are inorganic ceramic materials, which withstand very high temperatures and do not change their properties (a priori).

Figure 2: Carbo Accucast ID50; SiC; silica sand

Carbo Accucast ID50 is a ceramic proppant. A proppant is a synthetic solid material designed to keep an induced hydraulic fracture open, and is applied in fracking technologies, where it is added to a fracking fluid. *CARBOACCUCAST® ID50* is the proppant selected for this study. This material was provided by *Carbo Ceramics.* According to *Carbo Ceramics, CARBOACCUCAST®* is a sintered ceramic engineered with mullite and corundum crystals, which generate high hardness and durability that allows particle breakdown to be resisted. Furthermore, it is engineered with high roundness and sphericity and is chemically inert [18].

The **silica sand** used comes from a mine in Segovia, located in the autonomous community of Castilla and León, Spain (from the *Sachonuño* mine). This sand of mineral origin was provided by *Silices de Segovia*, a company dedicated to the sale and supply of siliceous sand of different particle size for use mainly in artificial sports grass. Before the sample arrived, it went through a process of extraction, wet screening, washing exclusively with water, and drying to remove the biomass and dry screening. According to the supplier, the approximate SiO_2 content is between 91% and 97% in the standard mines and may vary depending on the extraction zone.

The **SiC** used was provided by Panadyne. This material is produced by heating silica sand and a carbon source, usually petroleum coke. After that process, Silicon carbide may have two different colours depending on the purity, black or green. The material used is Black Silicon Carbide (98.5%-99.3% of purity), which is less pure than the green variety. Silicon Carbide is characterised by its properties, such as high hardness, chemical inertness, high thermal conductivity, and abrasion resistance, low coefficient of thermal expansion, thermal shock resistance and strength at high temperature ranges.

2.2. Physical and thermal treatments

Thermal aging

As mentioned above, temperatures can reach over 1000ºC in a central receiver. Hence, it is important to ensure the particle media can withstand these temperatures during extended periods of exposure (the worst-case scenario).

Therefore, to determine whether the selected solid particles materials are able to reach the desired temperature, they underwent an aging treatment, which consists of leaving the samples in the furnace at 900ºC for 500 hours and then letting them cool at room temperature with a moderate cooling rate.

Fluidization

Figure 3 shows a scheme of the experimental facility. It shows the fluidized bed used in these tests, which consists of a cylindrical bed of 8 cm of diameter filled with solid particles, with a bed aspect ratio (ratio between the height and the bed diameter) of approximately 1. At the top of the scheme, at approximately 1.5 m from the bed distributor, a short-arc ozone-free 4 kWel Xe lamp is located to simulate the concentrated solar energy, although the Xe-lamp was not used in this work. To carry out this work and to fluidize the bed of particles, an inlet air supply is necessary. In these tests, a compressor CEVIK PRO with an operating pressure of 10 bar produces the air supplied for the fluidization. The air enters at the plenum and then flows into the bed through a distribution plate with a thickness of 1 mm, which presents 44 perforations with a diameter of 1 mm, which ensure uniform distribution of the air in the cross section of the bed. The electric heaters were disconnected for these tests. Once the air enters from the bottom part of the bed, it comes into contact with the particles (fluidizing solid particles). The bed is equipped with several sensors and thermocouples to measure the pressure and the temperature inside the facility. The thermocouples and the pressure sensor are connected to a data acquisition system to record and save the data.

The fluidization tests entail fluidizing solid particles in the bed for 250 hours at twice the minimum fluidization velocity. The motion of the particles, which are in continuous operation, produces the abrasion and erosion of the particles.

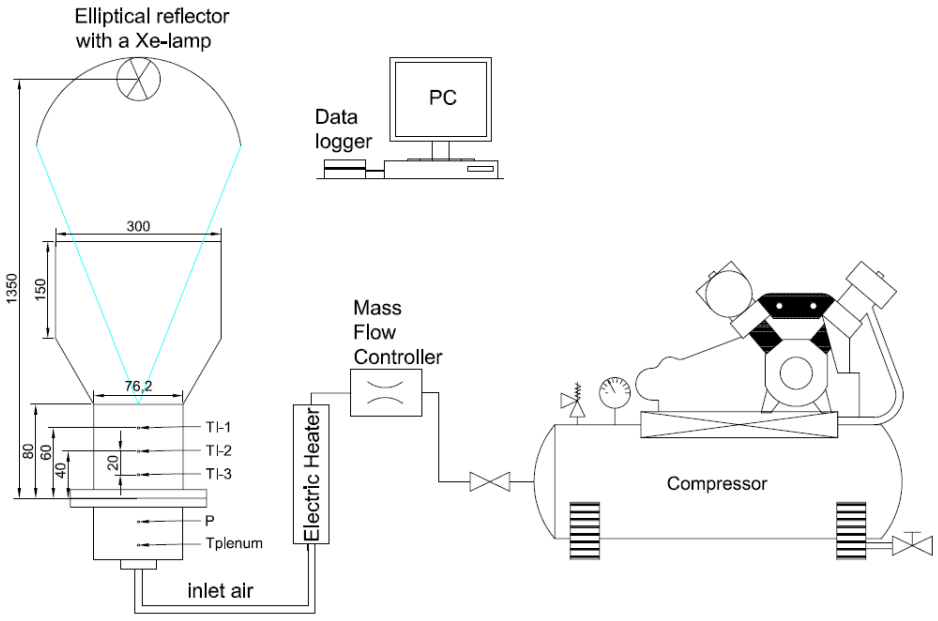

Figure 3: Scheme of the experimental facility used in this work for the fluidization tests. Dimensions in mm.

3. Methodology

In this work, 12 samples were analysed, with 4 different samples being studied for each material:

1) Initial sample: material as supplied.

2) Aging sample: Sample subjected to thermal aging, leaving a sample at 900ºC for 500 hours.
3) Fluidization sample: the solid particles of this sample were fluidized for 250 hours at twice the minimum fluidization velocity (at ambient temperature).
4) Aging +fluidization sample: This sample was subjected to both treatments. First, the sample was heated in a furnace at the same condition as the aging sample and, in a second step, this material was fluidized as in the previous sample conditions.

All the methods set out below are intended to identify the particles' density, thermal resistance and mechanical abrasion resistance, their optical properties, change in their chemical composition and the minimum fluidization rate of each material before (Sample 1) and after each treatment (Samples 2, 3 and 4), without sifting.

3.1. Physical and morphological characterization

Density

The real density of each solid particle material under study was characterized with a previously calibrated Helium Pycnometer Micrometrics Accu-Pyc 1330. This device measures the real volume of a solid when a known Helium volume is expanded into a chamber containing the sample and the same chamber without the sample. Consequently, the real volume obtained includes no pore volume accessible to the gas and the sample mass is previously weighted, so the density is directly calculated.

Particle Size Distribution (PSD)

This was determined with a Beckman Coulter LSTM 13 320 laser diffraction particle size analyser with Universal Liquid Module using Electrical Sensing Zone Method for Particle Size Distribution (PSD) analyses. It is important to know the particle size distribution in order to optimize the receiver thermal efficiency and to avoid sintering. Therefore, changes in PSD suggest breakage and/or wear of the particle during the treatments and the treatments described are not expected to cause significant changes in the PSD of the particles.

Scanning Electron Microscopy (SEM)

Particle morphology and surface changes were characterized by scanning electron microscopy (SEM; FEI Quanta-200). As the treated materials are not electric conductors, they were coated with graphite. The geometry and characteristics of the surface of the different materials were studied, observing the superficial damage of the particles submitted to the different treatments.

3.2. Thermal properties

Due to the high temperatures to which particles are exposed, thermal properties are key properties to be characterized. Given the importance of the values of the thermal properties, any changes that affect them after the described treatments will be analysed.

Differential Scanning Calorimetry (DSC)

In general terms, DSC applies a heating rate simultaneously to the sample and the reference crucibles. The temperatures of both cells are increased identically at the same time. The difference in the input of the energy required to match the temperature of both crucibles (sample and reference) is the amount of excess heat absorbed or released by the sample.

The DSC measurements were performed at 400 ºC. Around 25 mg of the selected sample was placed inside a 40 µL aluminium crucible under 50 mL·/min^{-1} N_2 flow and the measurements were calibrated with 25 mg sapphire. The device used was a DSC822e from Mettler Toledo and the method used was that described in a previous work [20].

3.3. Optical properties

Absorptance

In the opened free-falling particle receiver configuration, particles fall down at considerable speed. This means that the residence time of the particles inside the receiver is short. Consequently, the particles are required to have high absorptance properties.

The spectrophotometer used to perform the absorptance measurements was the Perkin Elmer lambda 950 with a 150 mm integrating sphere, where one beam of every wavelength is launched with the desired accuracy (5 nm in this case) until the most significant range of the solar spectrum is completed. This range goes from 300 nm to 2500 nm. To measure solar absorptivity, the wavelengths measured in this study were weighted following AM 1.5 [12]. This number represents the spectrum at mid latitudes, corresponding to places where at midday the solar incident angle value is 48.2º.

3.4. Chemical composition

During the treatments implemented in this study, the particles undergo harsh conditions. It is important to have information on chemical compositions and the crystalline phases in the samples, with a view to understanding the changes generated by the treatments.

X-Ray Diffraction (XRD)

The crystallographic structure of the materials was characterized by X-ray diffraction (XRD) in a diffractometer from Philips MRD. XRD is one of the most efficient techniques to perform quantitative and qualitative analysis of materials crystalline phases [21]. As the XRD pattern of a substance is considered the "fingerprint" of the substance [22], if the different treatments affect or produce changes in the crystalline phases, they can be analysed using this characterization technique.

3.5. Minimum fluidization velocity (U_{mf})

Minimum fluidization velocity is a key parameter in the fluidization field, and is defined as the minimum airflow rate needed to overcome the weight of the particles in the bed. This parameter depends on the size, density and geometry of the particles, and is thus a characteristic of each material. Hence, the minimum fluidization velocity of each material is a key parameter to be determined. Therefore, the minimum fluidization velocity was experimentally measured, following the procedure suggested by different authors [23-24].

This experimental procedure is focused on obtaining the intersection point (U_{mf}), generated by the linear tendency of the pressure drop profile of the bed with particles along the different airflow rates and the horizontal line, which is the pressure drop generated by the mass of particles. The pressure drop of particles can be calculated as follows:

$$\Delta P_{mass} = \frac{m \cdot g}{\frac{\pi}{4} \cdot D^2}$$

Where the numerator corresponds to the weight of particles and the denominator is the bed area. According to several authors [24], the pressure drop across the bed of particles ($\Delta P_{particles}$) can be obtained by subtracting the total pressure drop of the system when the bed has a mass of particles inside ($\Delta P_{system+particles}$) and the pressure drop when the bed is empty (ΔP_{system}) [26].

$$\Delta P_{particles} = \Delta P_{system+particles} - \Delta P_{system}$$

4. Results

Table 1 summarizes the main properties analysed in this work. From these results, it can be highlighted that to achieve the same storage capacity ($m \cdot Cp$) for the three materials, the mass of sand would be less than that of carbo and SiC since it presents the highest specific heat.

Table 1: summary of the main properties analysed for the solid particles.

	$\boldsymbol{\rho}$ $(\mathbf{kg/m^3})$	$\boldsymbol{\rho_{bulk}}$ [1] $(\mathbf{kg/m^3})$	$\boldsymbol{c_p}$ $(\mathbf{kJ/(kg \cdot K)})$	**d90** $(\boldsymbol{\mu m})$	**Absorptivity (-)**	$\mathbf{U_{mf}}$ $(\mathbf{m/s})$	**Cost** [2] $(€/\mathbf{kg})$
Sand	2630 ± 40	1450	1.05 ± 0.01	465.3 ± 1.4	0.44 ± 0.05	0.08 ± 0.01	0.44
SiC	3220 ± 140	1770	1.27 ± 0.01	406.2 ± 1.5	0.90 ± 0.01	0.09 ± 0.01	2.40
Carbo	3350 ± 210	1810	1.08 ± 0.01	354.6 ± 0.6	$0.95 \pm 0.01.4$	0.10 ± 0.01	1.70

The values shown are for the initial sample cases (Table 1).

[1]Bulk density, data from the supplier

[2]The costs were calculated according to the price of the material when ten tonnes are bought (Table 1).

One of the key aspects when selecting a material for CSP applications is for it to have adequate optical properties. In this case, the absorptivity of the three materials was studied and a clear advantage was detected in the absorptivity values of Carbo and SiC with respect to the sand, as is explained in Section 4.4. However, the costs of these two materials is 4-5 times higher than that of sand. Therefore, the good behaviour of Carbo (resistant to temperature and abrasion) and its adequate optical properties (high absorptivity) in the four samples reveals the great potential of Carbo for use in CSP applications. Its main drawback is its high density, which entails a higher pumping cost to move or fluidize carbo particles.

In view of the summarized results presented in Table 1, it is not straightforward to choose only one material. It would be necessary for an actual, industrial-scale application to perform a detailed energy and economic analysis. It is necessary to determine whether the higher thermal efficiencies to be, presumably, reached by SiC and Carbo (due to their higher absorptivities), compensates for the higher pumping cost of fluidizing them, due to their higher densities and higher minimum fluidization velocities.

In addition, the cost per kg of sand is much lower than that of SiC and Carbo. In summary, the sand could be the most suitable material from an economic point of view (lower pumping and material costs). SiC and Carbo could obtain higher thermal efficiencies and absorb more solar energy due to their high absorptivities. It is necessary, for each application, to perform a detailed economical study to determine whether the higher efficiency of the system compensates for the higher cost of SiC and Carbo.

4.1. Minimum fluidization velocity

The first step in the fluidization tests was to obtain the minimum fluidization velocity of each material. Figure 4 shows the experimental minimum fluidization velocities of the three materials at ambient temperature, which was maintained between 22 and 24 ºC during experiments. Specifically, the lines denominated “bed of sand”, “bed of SiC” and “bed of Carbo” show the pressure drop in the bed versus airflow rate. The dotted horizontal lines represent the pressure drop generated by the mass of particles in the bed, i.e. the weight of the mass of particles divided by the cross section of the bed. The intersection point between the solid and the horizontal lines provides the minimum fluidization volumetric flow rate of each material. Using the airflow rate, the minimum fluidization velocity is calculated. According to Figure 4, the minimum fluidization airflow rate for sand, SiC and Carbo is 24.51 l/min (0.08 m/s), 28.27 l/min (0.09 m/s) and 30.51 l/min (0.10 m/s), respectively. The minimum fluidization velocity of a granular material increases with its density and with particle size [23]. In the three materials tested in this work, the higher density of the Carbo has a greater influence on the minimum fluidization velocity than its lower size. As a result, the highest velocity was obtained for the Carbo. It is important to highlight that, in CSP applications, this airflow rate influences the pump costs, which may be relevant when choosing a material. Thus, this small difference in the airflow rate needed to fluidize the particles between three materials might be an important parameter to consider in a real set-up.

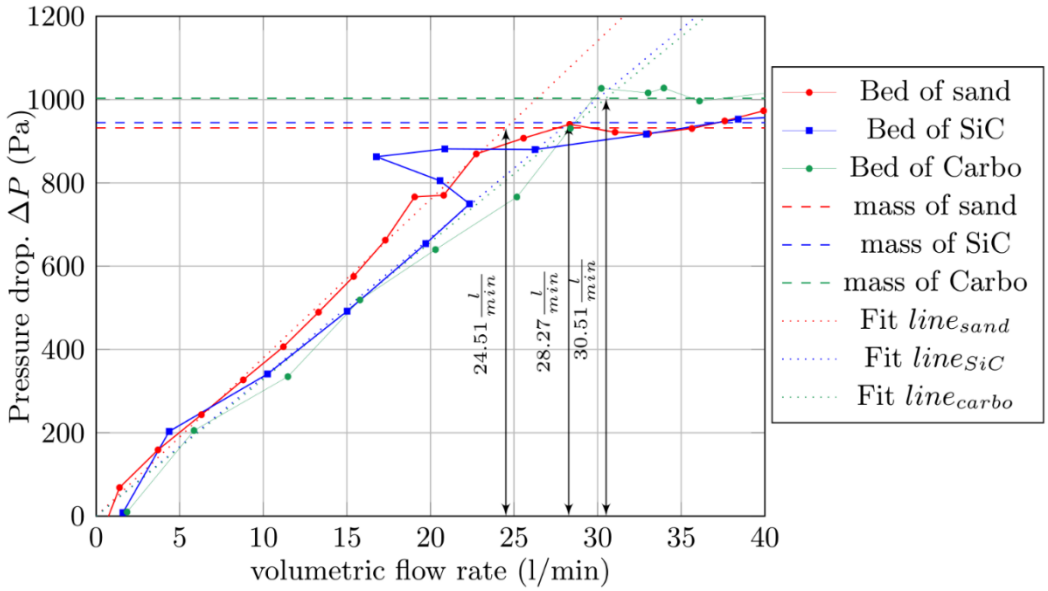

Figure 4: pressure across the bed at different superficial airflow rates for sand, SiC and Carbo

In an actual CSP application with higher temperatures (above 1000 ºC), the minimum fluidization velocity may vary due to the change in the air density. Several works [33, 34] have shown that the minimum fluidization velocity tends to decrease slightly with increasing temperatures, which should be taken into account when working at high temperatures.

4.2. Physical analysis

Two physical parameters are obtained: density and d90 parameter from PSD. Both density and bulk density are shown in Table 1, where it can be seen that the carbo is the densest material on both density measurements. Using the particle size distribution, the d90 parameter was obtained, which indicates that 90% of the sample has particles with a diameter bellow this value in a volumetric distribution. The values of d90 are summarized in Table

1, and Figure 5 shows their variation for the treatments proposed in each of the samples: the initial sample, the initial sample after the aging process, the initial sample after the fluidization process and the initial sample after the aging and the fluidization process.

Figure 5 corroborates the stability in particle size shown by the SiC and the Carbo after the aging test, unlike the sand. It is also worth noting the increase in particle size after fluidization tests. This can be attributed to particle agglomeration, where the case of SiC can be highlighted. The figure includes the standard deviations as error bars for each case. Initial and aged samples show a small deviation, i.e. d90 measurements were homogeneous. However, the fluidization samples show that d90 had a high variation, with the sand sample specifically presenting the highest standard deviation value ($\pm 36.2\ \mu m$), which may be attributed to the production of fines during fluidization. It can be highlighted that the combination of both tests (aging +fluidization) fails to contribute significantly to the agglomeration of the different particles tested.

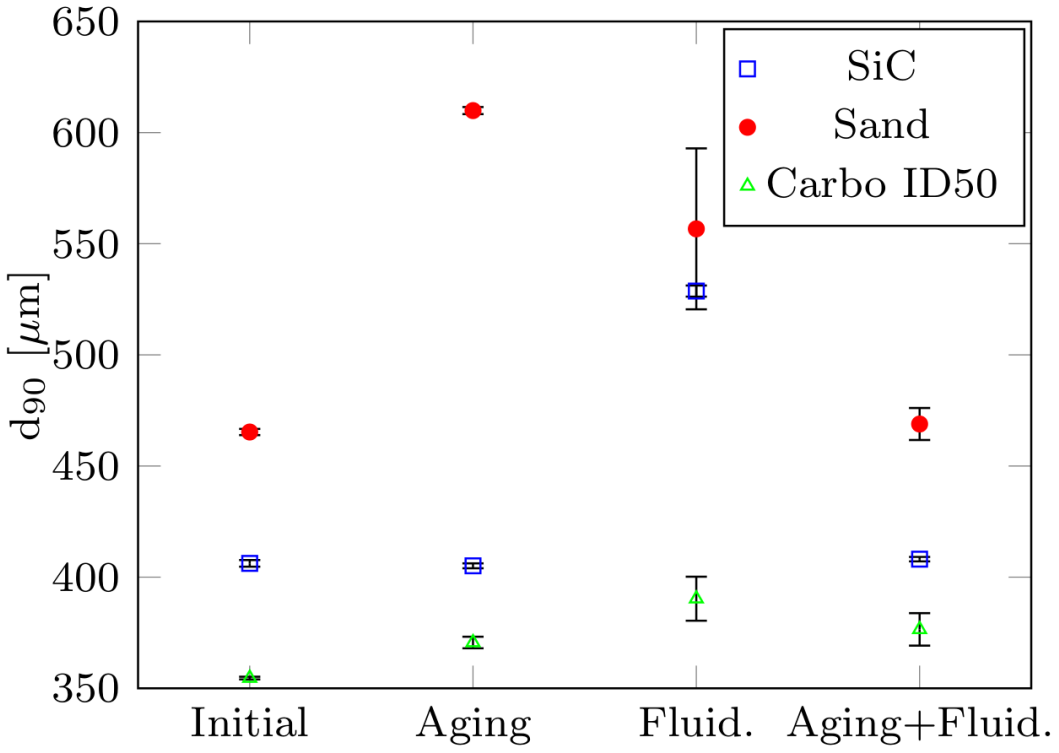

Figure 5: d90 sample values with error bars.

4.3. Thermal properties

The Cp was measured in order to understand the potential of each material to be used as a thermal energy storage medium and the main results are shown in Figure 6. The Cp changes between 5-8% across the thermal, mechanical and combined treatments. The Cp slightly increases with thermal aging treatment (up to 4%) for Carbo and sand samples, while it slightly decreases (up to 8%) for the SiC sample. Likewise, fluidization has no significant influence on the Cp. Therefore, as a conclusion, none of the three tested materials varies their energy storage capacity significantly under the experimental conditions tested in this work.

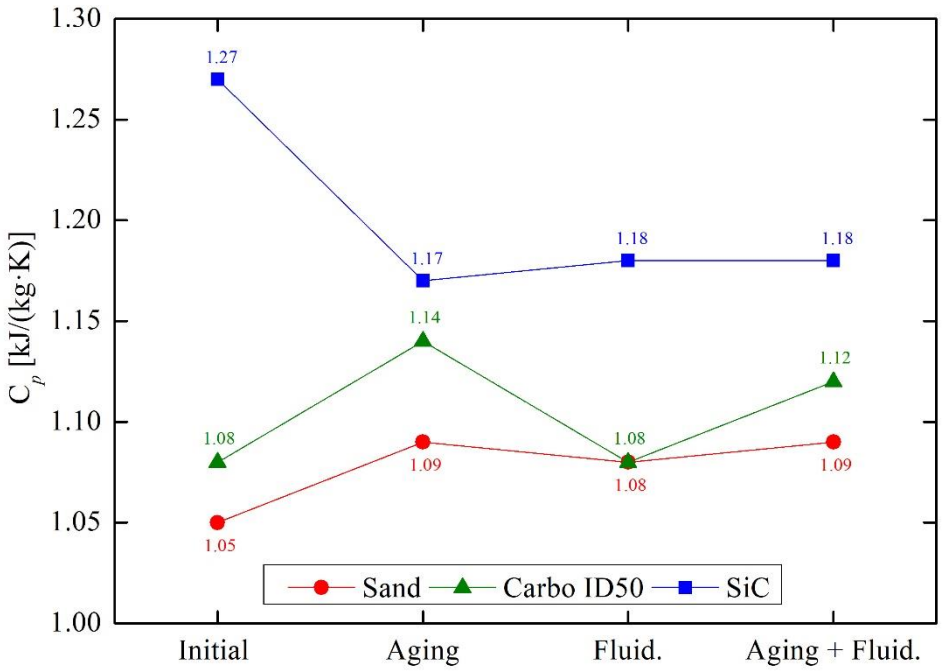

Figure 6: specific heat versus treatments. Equipment error: $\pm 0.01\ kJ/(kg \cdot K)$

Other works have presented results for the specific heat of the same materials at higher temperatures. For example, Ho et al. [35] proposed that the specific heat of Carbo can be obtained with the following expression:

$$Cp = 350 \cdot T^{0.18}$$

With the temperature in Celsius degrees, this correlation is valid for temperatures from 50 to 1100 ºC. In this expression, for a temperature of 400 ºC, a specific heat of approximately 1030 J/(kg·K) is obtained. The numerical value is similar to that obtained experimentally in this work. Experimental error and origin of the supplied materials may lay behind the small differences. The specific heat capacity of sand and SiC is similar to that found by other researchers [17, 36].

4.4. Optical properties

The absorptivity results are shown in Figure 7. The absorptivity of the silica sand is the lowest measured in this study. This property is, however, able to achieve an increment of up to 50%. This is key if the required final

application is a direct-open CSP plant receiver for the final system. Moreover, the differences between the other two materials are also similar, achieving less than 5% increments, if any.

SiC and Carbo have higher absorptivity, with Carbo Accuscast ID50 being that with the highest absorptance properties with the highest values after the combined thermal treatment (more than 95% absorptivity). The variation in the absorptivity measures conducted in each case is negligible.

This property is crucial for open-direct systems to be installed in CSP plants and, hence, all the materials studied here can be used, except the silica sand because this solid particle presents very low absorptivity. However, it could be the most promising solution for many other CSP configurations that appear in CSP databases.

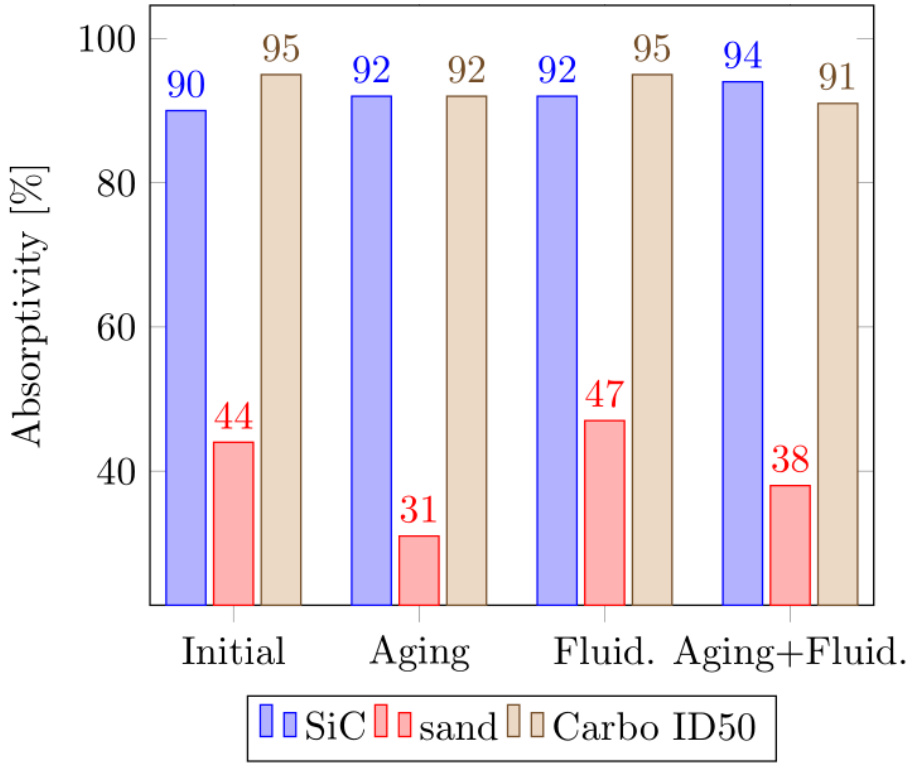

Figure 7: absorptivity diagram with data for 4 samples for sand, SiC and Carbo.

4.5. Chemical composition

Figure 8 shows the X-Ray diffractograms obtained for each solid and each treatment. The crosses (and squares) mark the main peaks that identify a crystalline substance. First, the silica sand from Segovia is identified as having the crystalline structure of quartz when analysing the main components Figure 8a). It is known that silica sand may have minor impurities in its composition, but these are below the XRD technique detection limit. Moreover, the X-Ray patterns of the four different silica sand samples almost overlap, revealing there are no significant changes in the crystalline structure under the treatments. Figure 8 b) shows silicon carbide has SiC as main crystalline phase. Similarly, there are no significant changes under the treatment. Carbo Accucast ID50 is composed of two major crystalline phases, namely, aluminium oxide and mullite. In this material, when applying both treatments (aging and fluidization), the baseline may suggest an increase in amorphous content, indicating that these treatments affect the crystallinity of the solid.

a) Silica sand

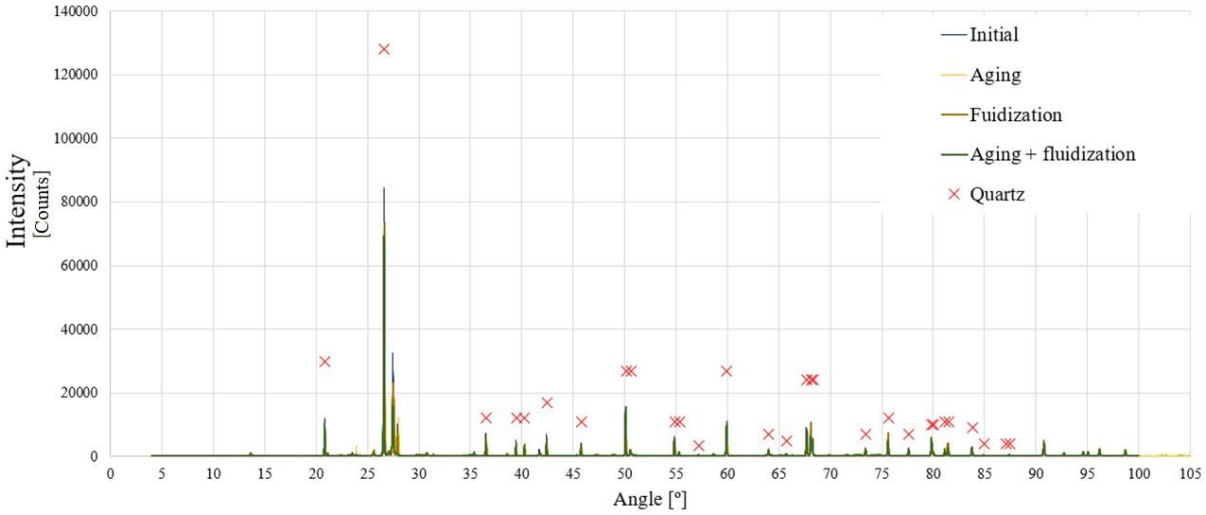

b) SiC

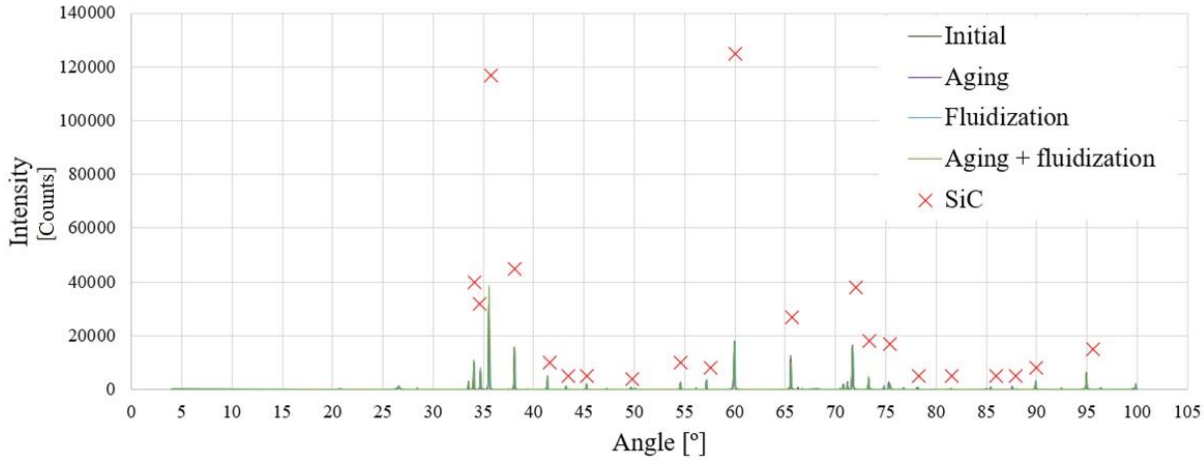

c) Carbo ID50

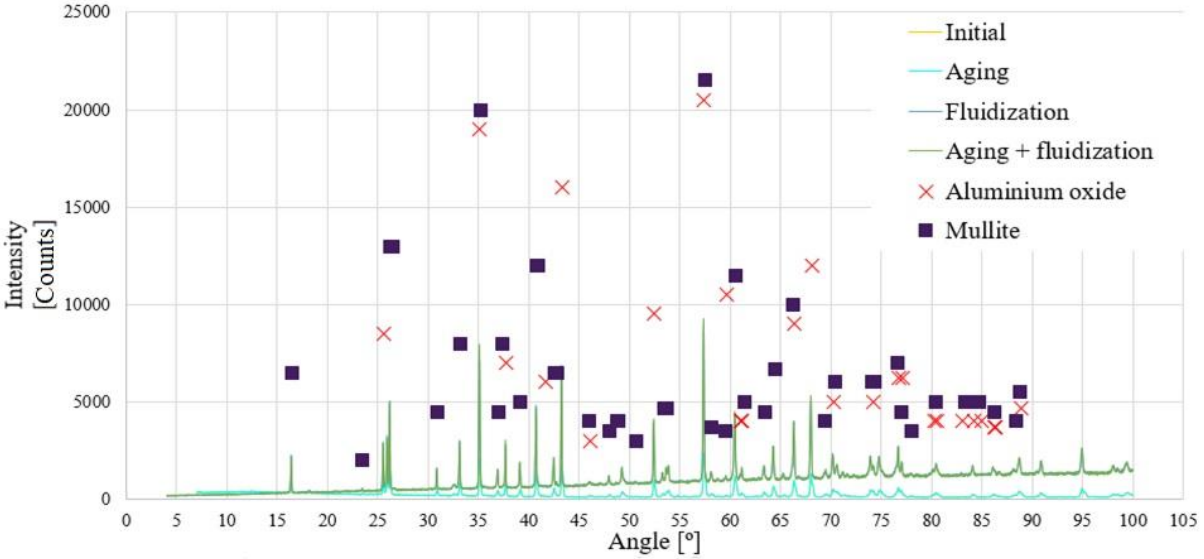

Figure 8. XRD results of the sample under study considering the initial, aged, fluidized and aged+fluidized samples: a) Silica Sand; b) SiC; c) Carbo Accucast ID50.

4.6. Imaging analysis

The SEM images of the samples under study are shown in Figure 9. Despite being a qualitative observation, some superficial wear is observed, especially in the edges of the particles in the images of the fluidized samples of sand and SiC. Moreover, the fluidized sand particles show small particles on the surface, probably due to the production of fines during fluidization. This result is consistent with the d90 measurements and standard deviations for the fluidized sand sample and, to a lesser degree, the aged and fluidized sand sample.

	Initial	Aged	Fluidized	Aged + Fluidized
Silica Sand	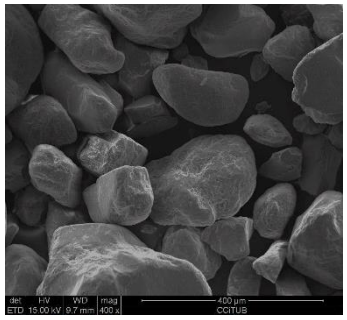	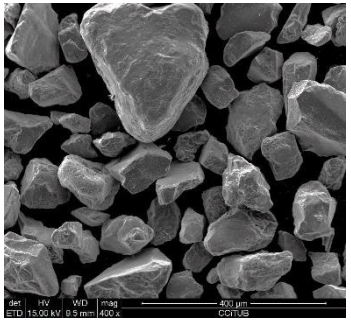	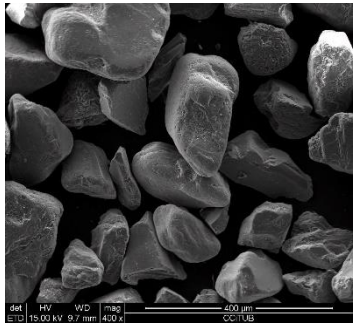	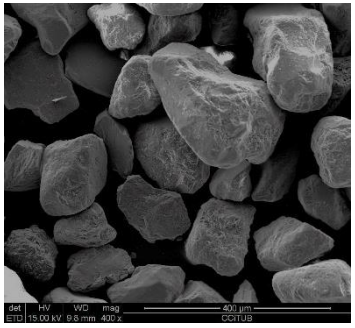
SiC	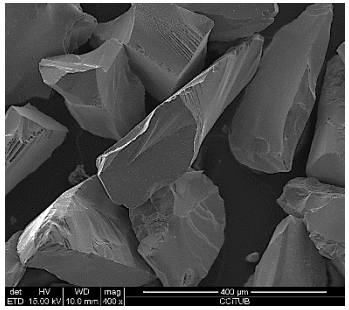	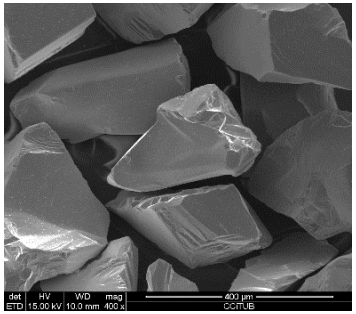	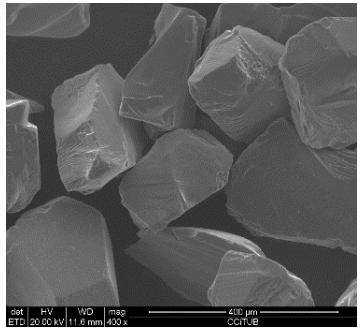	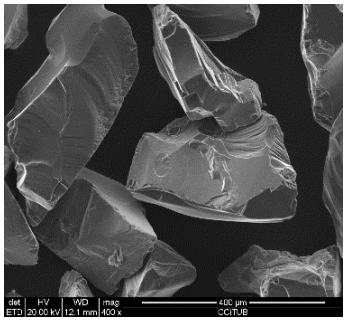
Carbo ID50	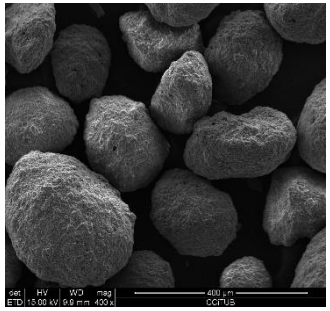	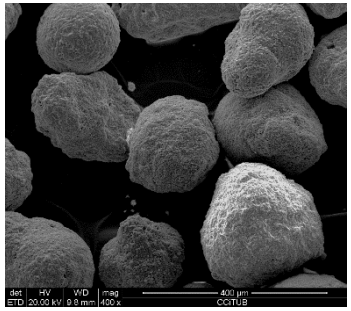	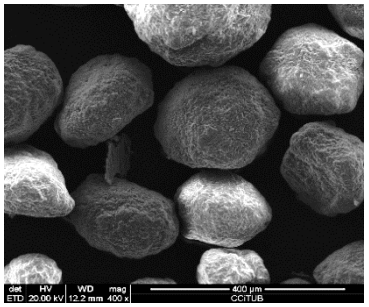	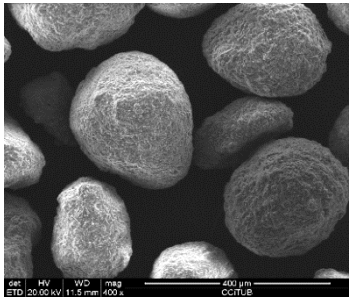

Figure 9. SEM images obtained for the samples under study when the mechanical, thermal, and combination of both tests are applied.

5. Conclusions

The three granular materials tested in this work show good resistance to the fluidization process and are stable at high temperatures over long periods of time. There is no significant change in their chemical composition and their energy storage capacity (specific heat) and absorptivity did not vary notably after the tests. The main attractive property of SiC and Carbo is their very high absorptivity, which is around or over 0.9, while for the sand it is around 0.4. This ensures a higher capacity of absorbing direct solar radiation on them, increasing the temperature and the efficiency of the system. In contrast, sand is an abundant material in regions of the planet with high levels of solar radiation [25] and is 4-5 times cheaper than SiC and Carbo. Furthermore, its lower density permits sand particles to be transport / fluidized with lower pumping costs.

Particle size distribution analysis showed great variation in d90 measurements for the silica sand particles after being fluidized. This was attributed to the appearance of fines, which was later confirmed with the observation through SEM.

Future work is needed to test the same materials during a cycling process of heating-cooling at elevated temperatures in a fluidized bed, to corroborate the suitability of these materials for actual CSP applications. The combination of the fluidization + thermal cycling should be studied.

Detailed economic analysis of a CSP plant with granular material is necessary to determine whether the better thermal properties of SiC and Carbo and the higher efficiency reached compensate for the materials' higher costs. The properties and results presented in this work are necessary for the decision-making process.

6. Acknowledgement

This work was partially funded by the Spanish Ministry of Economy and Competitiveness RTI2018-093849-B-C32 and ENE2016-78908-R (MINECO/FEDER), by the Agencia Estatal de Investigación (AEI) of the Ministerio de Ciencia, Innovación y Universidades (RED2018-102431-T), by the regional government of Castilla-La Mancha (SBPLY/17/180501/000412). The authors would like to thank the Catalan Government for the quality accreditation given to their research group (DIOPMA 2017 SGR 0118). DIOPMA is a certified agent TECNIO in the category of technology developers from the Government of Catalonia.

References

[1] Bandyopadhyay, S. (2019). "The first step towards energy revolution." (2019), p 227-228.

[2] Li, M. (2017). World energy 2017-2050: *Annual report. Department of Economics, University of Utah*.

[3] International Energy Agency 2019 Renewables 2019. Available from: https://www.iea.org/statistics/renewables/ [Accessed: 10-07-2020].

[4] International Energy Agency (IEA). Technology Roadmap: Solar Thermal Electricity. 2014. [Online] Available from: http://www.iea.org/publications/freepublications/publication/TechnologyRoadmapSolarThermalElectricity_2014edition.pdf [Accessed: 26-09-2019].

[5] International Energy Agency (IEA). Status of Power System Transformation. Advanced Power Plant Flexibility. 2018. [Online] Available from: https://webstore.iea.org/download/direct/1041?fileName=Status_of_Power_System_Transformation_2018.pdf [Accessed: 02-07-2019]

[6] Almendros-Ibáñez, J. A., Fernández-Torrijos, M., Díaz-Heras, M., Belmonte, J. F., & Sobrino, C. (2019). A review of solar thermal energy storage in beds of particles: packed and fluidized beds. *Solar Energy*, 192, 193-237.

[7] Ho, C. K. (2017). Advances in central receivers for concentrating solar applications. *Solar energy*, *152*, 38-56.

[8] Ho, C. K. (2016). A review of high-temperature particle receivers for concentrating solar power. *Applied Thermal Engineering*, *109*, 958-969.

[9] Ho, C., Christian, J., Gill, D., Moya, A., Jeter, S., Abdel-Khalik, S. & Gobereit, B. (2014). Technology advancements for next generation falling particle receivers. *Energy Procedia*, *49*, 398-407.

[10] Yang, S., Wang, J., Lund, P. D., Jiang, C., & Li, X. (2019). High performance integrated receiver-storage system for concentrating solar power beam-down system. *Solar Energy*, *187*, 85-94.

[11] Díaz-Heras, M., Moya, J. D., Belmonte, J. F., Córcoles-Tendero, J. I., Molina, A. E., & Almendros-Ibáñez, J. A. (2019). CSP on fluidized particles with a beam-down reflector: Comparative study of different fluidization technologies. *Solar Energy*. In press.

[12] Calderón, A., Palacios, A., Barreneche, C., Segarra, M., Prieto, C., Rodriguez-Sanchez, A., & Fernández, A. I. (2018). High temperature systems using solid particles as TES and HTF material: a review. *Applied Energy*, *213*, 100-111.

[13] Kraemer, S. SolarPACES. (2018). *Particle Receivers to Get First Commercial Trial – in Saudi Arabia*. [Online]. Available from: http://www.solarpaces.org/particle-receiver-first-commercial-trial-2018/ [Accessed: 26-09-2019].

[14] Calderón, A., Barreneche, C., Palacios, A., Segarra, M., Prieto, C., Rodriguez-Sanchez, A., & Fernández, A. I. (2019). Review of solid particle materials for heat transfer fluid and thermal energy storage in solar thermal power plants. *Energy Storage*, *1*(4), e63.

[15] Palacios, A., Calderón, A., Barreneche, C., Bertomeu, J., Segarra, M., & Fernández, A. I. (2019). Study on solar absorptance and thermal stability of solid particles materials used as TES at high temperature on different aging stages for CSP applications. *Solar Energy Materials and Solar Cells*, *201*, 110088.

[16] Flamant, G., Gauthier, D., Benoit, H., Sans, J. L., Garcia, R., Boissière, B. & Hemati, M. (2013). Dense suspension of solid particles as a new heat transfer fluid for concentrated solar thermal plants: On-sun proof of concept.*Chemical Engineering Science*,*102*, 567-576.

[17] Diago, M., Iniesta, A. C., Soum-Glaude, A., & Calvet, N. (2018). Characterization of desert sand to be used as a high-temperature thermal energy storage medium in particle solar receiver technology. *Applied energy*, *216*, 402-413.

[18] Carbo Accucast. *Carbo – carbo ceramics & Technologies*. [Online]. Available from: https://www.carboceramics.com/about/about-carbo/Fracture-technologies-overview [Accessed: 26-09-2019].

[19] Krause, C., Eldred, B., & Canova, S. (2019). U.S. Patent Application No. 16/167,317.

[20] Ferrer, G., Barreneche, C., Solé, A., Martorell, I., Cabeza, L.F. (2017). New proposed methodology for specific heat capacity determination of materials for thermal energy storage (TES) by DSC. Journal of Energy Storage 11, 1-6

[21] CAI de Técnicas Geológicas." [Online]. Available from: https://www.ucm.es/tecnicasgeologicas/difraccion-de-rayos-x-drx . [Accessed: 28-04-2019].

[22] Instituto de Diagnóstico Ambiental y Estudios del Agua." [Online]. Available from: http://www.idaea.csic.es/index.php?option=com_ogngrups&view=detall_grup&Itemid=98&cid=46&lang=es . [Accessed: 28-04-2019].

[23] Kunii, D., & Levenspiel, O. (2013). *Fluidization engineering*. Elsevier.

[24] Kathuria, D. G., & Saxena, S. C. (1987). A variable-thickness two-dimensional bed for investigating gas—solid fluidized bed hydrodynamics. *Powder technology*, *53*(2), 91-96.

[25] Diago, M., Iniesta, A. C., Soum-Glaude, A., & Calvet, N. (2018). Characterization of desert sand to be used as a high-temperature thermal energy storage medium in particle solar receiver technology. Applied Energy, 216, 402-413.

[26] Díaz-Heras, M., Barreneche, C., Belmonte, J.F., Calderón, A., Fernández A.I., Almendros-Ibáñez, J.A. (2020). Experimental study of different materials in fluidized beds with a beam-down solar reflector for CSP applications. Solar Energy, in press.

[27] Flamant, G., (1982). Theoretical and experimental study of radiant heat transfer in a solar fluidized-bed receiver. AIChE Journal 28 (4), 529-535.

[28] Flamant, G., Olalde, G., (1983). High temperature solar gas heating comparison between packed and uidized bed receivers. Solar energy 31 (5), 463-471.

[29] Almendros-Ibáñez, J.A., Fernández-Torrijos, M., Díaz-Heras, M., Belmonte, J. F., Sobrino, C., (2019). A review of solar thermal energy storage in beds of particles: packed and fluidized beds. Solar Energy 192, 193-237.

[30] Tregambi, C., Chirone, R., Montagnaro, F., Salatino, P., Solimene, R., (2016). Heat transfer in directly irradiated fluidized beds. Solar Energy 129, 85-100.

[31] Sánchez-González, A., Gómez-Hernández, J., (2020). Beam-down linear fresnel reflector: BDLFR. Renewable Energy 146, 802-815.

[32] Geldart, D. (1973). Types of gas fluidization. Powder technology, 7(5), 285-292.

[33] Guo, Q., Yue, G., Suda, T., Sato, J., (2003). Flow characteristics in a bubbling fluidized bed at elevated temperature. Chemical Engineering and Processing: Process Intensification 42 (6), 439-447.

[34] Subramani, H. J., Balaiyya, M. M., Miranda, L. R., (2007). Minimum fluidization velocity at elevated temperatures for geldart's group-b powders. Experimental Thermal and Fluid Science 32 (1), 166-173.

[35] Ho, C. K., Christian, J. M., Romano, D., Yellowhair, J., Siegel, N., Savoldi, L., & Zanino, R. (2017). Characterization of particle flow in a free-falling solar particle receiver. Journal of Solar Energy Engineering, 139(2).

[36] Lalau, Y., Faugeroux, O., Claudet, B., Guillot, E., Andre, D., Huger, M. & Chotard, T. (2019). A method for experimental thermo-mechanical aging of materials submitted to concentrated solar irradiation. Solar Energy Materials and Solar Cells, 192, 161-169.